Parametric Modeling and Optimization of Switched Reluctance Motor for EV

Lijun Liu[1,2], Yu Huang[2], Mingwei Zhao[1,2*], and Yi Ruan[1]

[1]School of Electromechanical Engineering and Automation
Shanghai University, Shanghai, 200444, China
xznu_llj@163.com, xznu_zmw@163.com

[2]School of Electrical Engineering and Automation
Jiangsu Normal University, Xuzhou, 221116, China
1819931958@qq.com, yraun@mail.shu.edu.cn

***Abstract* –** To meet the high- performance requirements of new energy vehicle drive, the optimization design of 8/6 Switched Reluctance Motor is realized based on finite element parametric modeling of the motor. Firstly, the initial design of motor structure parameters is carried out based on the mathematical model of Switched Reluctance Motor, and the simulation model of the motor is built using RMxprt platform, and the debugging of the characteristics of the wide speed range of the motor is finished. Then, the parametric finite element model of the motor is generated, and the stator and rotor pole arc coefficients of the motor are selected as the optimization variables, and the multi-objective compromise optimization of the torque characteristics and efficiency of the motor is carried out by using the Quasi-Newton method weighting method. Finally, the magnetic field distribution, torque characteristics, efficiency and speed range characteristics before and after optimization are compared, proving that the optimized Switch Reluctance Motor can achieve multi-objective performance optimization. The motor designed by this modeling optimization method can improve the requirements of vehicle driving better.

***Index Terms* –** multi-objective performance optimization, parametric finite element modeling, Switched Reluctance Motor, wide speed regulation characteristics.

I. INTRODUCTION

In order to meet the requirements of various working conditions of new energy vehicles, the drive system has higher performance requirements. Switched Reluctance Motor (SRM) has the advantages of large starting torque, wide speed range, strong load capacity, high operation efficiency and high reliability [1], making it one of the best driving options for electric vehicles. However, due to its double salient pole structure and magnetic saturation nonlinearity, the torque pulsation is large. In addition, there are still high losses such as iron core loss and copper loss, which reduce the operating efficiency of the motor [2]. Therefore, it is necessary to further improve the modeling accuracy of SRM and optimize its electromagnetic performance.

A parameter analysis model of the motor should be established first to optimize the performance of the motor drive system. Look-up data tables-based modeling of SRM was realized by Memon et.al [3], but the storage of magnetization curve data requires a lot of hardware resources. The function fitting method [4] adopted the appropriate functional analytical formula to fit or model the relationship between flux or torque, phase current, and rotor position according to the modeling accuracy in practical application, but the parameters must be optimized and determined based on the family of magnetization curves obtained from experiments and finite element analysis. In [5], SRM rapidly converged to the optimal design in different aspects such as loss, cost, and weight with the help of Magnetic Equivalent Circuit (MEC) analysis;, the MEC method was fast, but it involved the assumption of magnetic flux, so the calculation results may not be accurate. Although the computation time of Finite Element Analysis (FEA) [6] was long, it could realize higher precise multi-physical domain simulations such as electric, magnetic, and noise, and comprehensively test and optimize the performance of the motor and drive system.

In addition, the optimization of motor model parameters is one of the effective methods for realizing motor performance optimization. In [6–8], the torque ripple and efficiency optimization of SRM was realized based on the finite element method, but the power speed range was not considered. Three evaluation indexes of SRM performance for electric vehicles were proposed, and the performance of motors such as torque, copper loss, and torque ripple was optimized by a multi-objective control

strategy in [9]. However, only the influence of turn-on and turn-off Angles on performance was considered, and the influence of structural parameters of the motor on performance was not considered.

An 8/6 structure SRM model suitable for a new energy vehicle drive system is designed based on the finite element parametric modeling method in this paper. Quasi-newton method and weighting method are used to optimize the efficiency, torque, and torque ripple of the motor. The comparison of motor performance before and after optimization proves that the optimized motor model can achieve the comprehensive optimization of torque ripple, speed range, and lose efficiency.

II. MATHEMATICAL MODEL OF SRM

SRM operates on the principle of least reluctance, where the flux closes according to the magnetic circuit with the lowest reluctance [10]. Due to the non-uniform distribution of the flux at the end of the motor, the non-linearity of the flux density, and the depth saturation of the magnetic circuit, the parameters of the flux Ψ, inductance, L and current i of the motor phase winding will change periodically with the rotor position angle θ and meet the nonlinear relationship. According to the theory of electromagnetic field, the conversion relationship between electrical, magnetic, and mechanical energy of SRM is presented [11]. It can be expressed by the following equation.

A. Circuit equation

Assuming that the four-phase structure of the motor is symmetric, the balance equation of Phase K is:

$$U_k = R_k i_k + \frac{d\Psi_k}{dt}, \qquad (1)$$

where U_k, R_k, i_k, and Ψ_k are the applied voltage, resistance, current, and flux of the K- phase winding.

The phase inductance $L_k(i_k, \theta)$ is a function of the phase current i_k and the rotor position angle θ due to the double salient pole structure of the SRM and the saturation effect of the magnetic circuit. Ignoring the hysteresis effect, eddy current effect, and phase-phase mutual inductance of SRM, the phase winding flux Ψ_k is the product of phase inductance $L_k(i_k, \theta)$ and phase current i_k, and the flux equation can be obtained as:

$$\Psi_k(i_k, \theta) = L_k(i_k, \theta)i_k. \qquad (2)$$

Take the derivative of the left and right sides of equation (2) and substitute it into equation (1) to get:

$$U_k = R_k i_k + i_k \frac{\partial L_k}{\partial \theta} \frac{d\theta}{dt} + (i_k \frac{\partial L_k}{\partial i_k} + L_k) \frac{di_k}{dt}. \qquad (3)$$

B. Electromechanical relation equation

As a speed regulating system, the key to the control of SRD is the control of electromagnetic torque, which is the electromechanical coupling term generated by SRM through the coupling magnetic field at the mechanical port. If the influence of mutual inductance between windings is not considered, the electromagnetic torque generated by the motor when one phase works independently is:

$$T_k = \frac{\partial W(i_k, \theta)}{\partial \theta} \mid i_k = const, \qquad (4)$$

where T_k is the instantaneous electromagnetic torque of one phase, and the magnetic common energy $W'(i_k, \theta)$ of the phase winding is expressed as:

$$W'(i_k, \theta) = \int_0^{ik} \Psi(i_k, \theta)di_k = \int_0^{i_k} L_k(i_k, \theta)i_k, di_k. \qquad (5)$$

Substitute equation (5) into equation (4) to obtain:

$$T_k = \frac{\partial W'(i_k, \theta)}{\partial \theta}\mid i_k = const = \int_0^{i_k} \frac{\partial L_k(i_k, \theta)}{\partial \theta}i_k di_k. \qquad (6)$$

The direction of SRM torque depends on the trend of the inductance curve, but has nothing to do with the direction of the current.

The total electromagnetic torque T_e of SRM can be obtained by:

$$T_e = \sum_{k=1}^{m} T_k. \qquad (7)$$

where m is the phase number of the motor.

C. Mechanical equation

According to the relevant mechanical knowledge, the mechanical equation of the rotor can be expressed as:

$$J\frac{d\varpi}{dt} = T_e - T_L - D\varpi, \qquad (8)$$

where ϖ is rotor angular velocity, and $\varpi = \frac{d\theta}{dt}$.

III. DESIGN AND ESTABLISHMENT OF SRM MODEL

In this design, the SRM rating parameters used in electric vehicles are set as shown in Table 1.

Table 1: Motor rating parameter settings

Parameter	Value	Parameter	Value
Rated speed (rpm)	1500	Rated output power (kW)	10
Voltage rating (V)	330	Operating temperature (cel)	120

A. Model parameters of motor initialization design

The selection of motor parameters is determined by the designer according to the motor performance and process production requirements, combined with their own design experience [12]. Table 2 lists the specific structural parameters of SRM.

In addition, the stator and rotor of SRM are made of silicon steel sheets laminated, and air gaps are unavoidable. Different silicon steel sheet materials have different magnetization curves, resulting in different magnetic

Table 2: SRM structural parameter

Parameter	Value	Parameter	Value
Number of stator	8	Number of rotor	6
D_{os} (Stator outer diameter) (mm)	240	D_{or} (Rotor outer diameter) (mm)	126.4
D_{is} (Stator inner diameter) (mm)	127.2	D_{ir} (Rotor inner diameter) (mm)	40
H_{cs} (Stator yoke height) (mm)	13	H_{cr} (Rotor yoke height (mm)	20
β_s (Stator pole arc) (deg)	21	β_r (Rotor pole arc) (deg)	21
Stator core length (mm)	140	Rotor core length (mm)	140
Winding turns (turns)	40	Advance conduction angle (degrees)	20
Upper and lower current (A)	80-78	Pulse width (deg)	110

load performances [13]. DW310_35 type silicon steel sheet is used in this design. Figure 1 shows its magnetization curve and the magnetic flux density B can be expressed as:

$$B = J + \mu_0 H, \qquad (9)$$

where J is the magnetization strength, μ_0 is the vacuum permeability, H is the magnetic field strength.
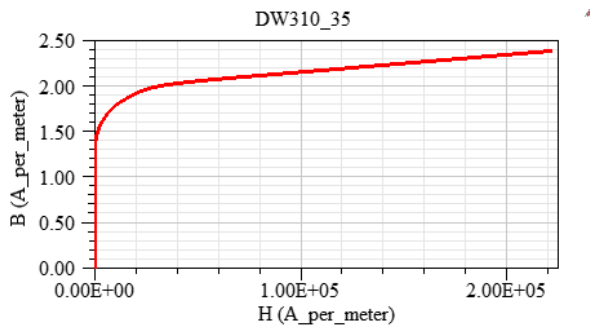

Fig. 1. Magnetization curve of silicon steel sheet DW310_35.

When the magnetic field intensity H reaches the order of 10^5, the magnetization curve enters the saturation phase. However, since the magnetic induction intensity $\mu_0 H$ in the space occupied by the medium doesn't saturate and rises slowly, the synthesized magnetization curve shows that B still increases slightly with the increase of H.

B. Establishment of SRM simulation model

After determining the parameters of each part, simulation modeling of the designed SRM is carried out as shown in Fig. 2 below.

The SRM simulation model established in RMxprt is shown in Fig. 2 (a), where the main structural parameters of the motor are marked. Figure 2 (b) is the 2D finite element model of SRM with mesh division imported into Maxwell. The rotation region and boundary of the model are respectively set, and the model is discretized by mesh division for a finite element solution.
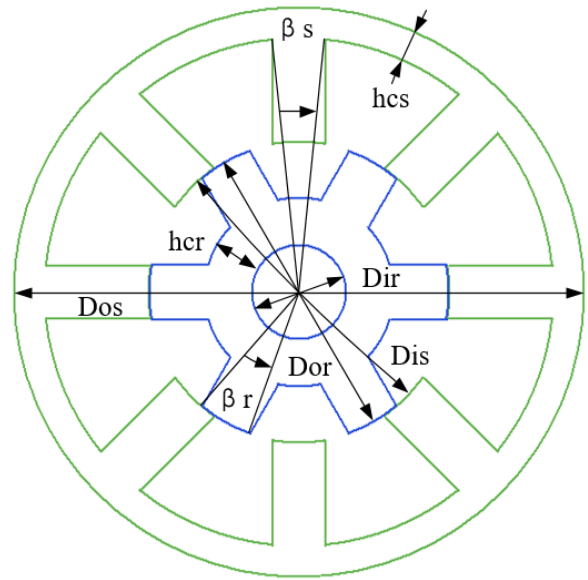
(a)
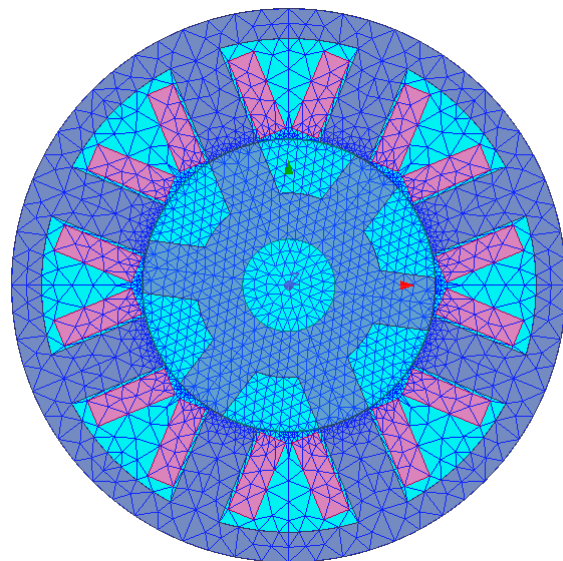
(b)

Fig. 2. Simulation model of SRM. (a) RMxprt simulation model. (b) Maxwell 2D finite element model.

IV. DEBUGGING OF SRM WIDE SPEED REGULATION CHARACTERISTICS

The speed control characteristics of SRM is shown in Fig. 3, where ω_r is the base speed of SRM and ω_{sc} is the highest speed in the constant power region [10]. Current Chopper Control (CCC) is used when the rotor angular velocity ω_r is in the range of $0 \sim \omega_b$, which makes the motor obtain the constant torque speed regulation characteristic. When ω_r is in the range of $\omega_b \sim \omega_{sc}$, SRM adopts Angle Position Control (APC), so that the motor can obtain constant power speed regulation characteristic. In addition, SRM works in series excitation characteristic when $\omega_r > \omega_{sc}$.
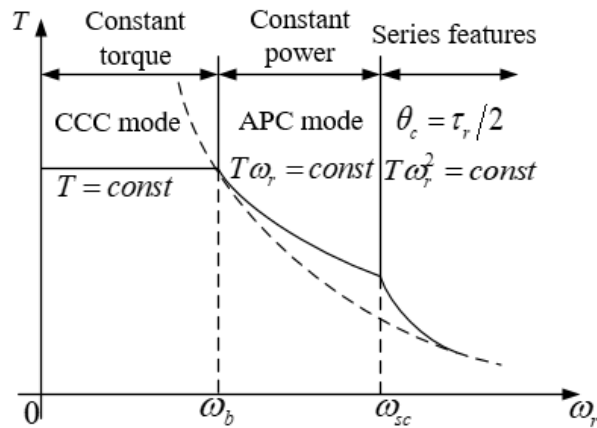

Fig. 3. Speed control characteristics of SRM.

A. Constant torque speed control characteristics below base speed ($0 < \omega_r < \omega_b$)

The rated speed of the motor is set as $\omega_b = 1500rmp$. CCC control is used and the upper and lower amplitude of the current is set to $80A\ 78A$ in the speed range of $0 < \omega_r < \omega_b$. The rated phase current and air gap inductance waveform of SRM below base speed is shown in Fig 4. The simulation results show that the output power is 9756.25 W and the rated torque is 62.1102 N.m, corresponding to excitation voltage $U_s = 330V$ and rated speed $\omega_b = 1500rmp$. The constant torque speed regulation characteristic of SRM can be achieved by maintaining. $U_s\omega_r$ during the debugging.

B. Constant power speed regulation characteristics above base speed ($\omega_b < \omega_r < \omega_{sc}$)

APC control is used above base speed, and the constant power characteristics can be achieved by adjusting the turn-on angle θ_{on} and the turn-off angle θ_{off} of the switch devices. The value of ω_{sc} needs to be determined first. It can be seen from the current waveform in Fig. 4 (a) that the abscissa electrical angle of the point m1, where the phase current drops to 0A, is

156°, and the abscissa electrical angle of the point m2, where the phase current begins to conduct in advance, is 340°. According to the torque waveform in Fig. 4 (b), the point m3, where the inductance rises to the maximum value, corresponds to an electric angle of 181° on the abscissa, while the point m4, where the inductance drops to 0 mH, corresponds to an electric angle of 316° on the abscissa. The current should be turned on at the moment when the inductance is 0 mH, so that the current reaches the maximum value before the inductance rises, and it should also fall to 0A before the inductance rises to the maximum value, so as to avoid negative torque of the motor [6]. Therefore, the angle corresponding to current conduction in advance can be further advanced by 25°, and the width of current can be further increased by 25°.
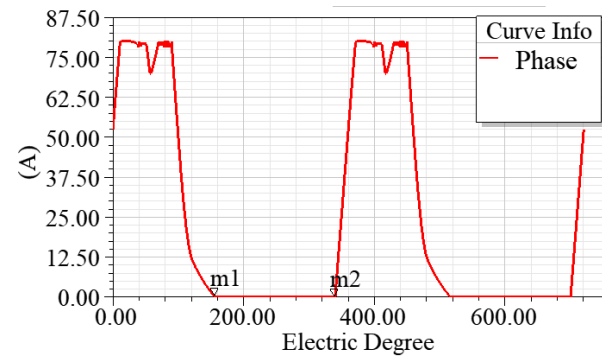
(a)
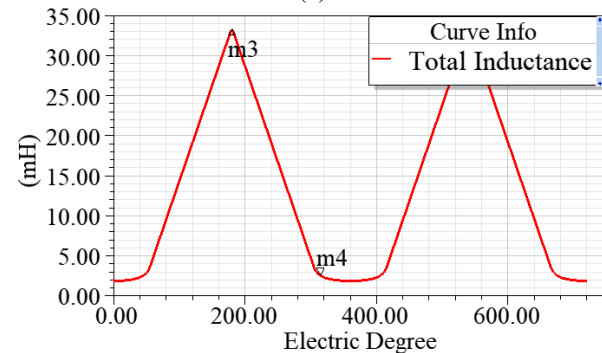
(b)

Fig. 4. Waveform of rated phase current and airgap inductance of SRM below base speed. (a) Rated current waveform of SRM below base speed. (b) Air gap inductance waveform of SRM below base speed.

According to the above conclusion, the advance conduction angle and opening width of the switch devices are adjusted accordingly. The simulation results show that, at that time of $\omega_{sc} = 6900rpm$, the output power is 9764.48 W and the output torque is 13.5136 N.m, that is, SRM can achieve the constant power operation characteristics in the wide speed regulation range of

1500rpm∼6900rpm. The phase current waveform of SRM corresponding to ω_{sc} is shown in Fig. 5.
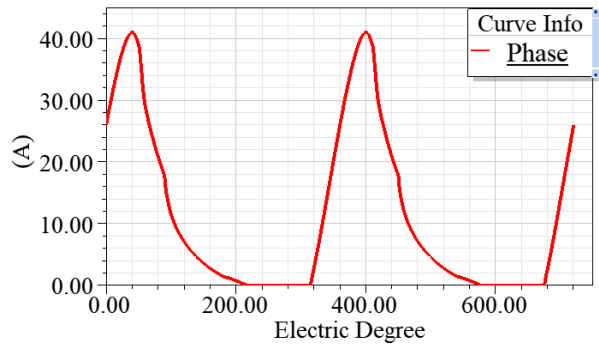
Fig. 5. Phase current waveform of SRM corresponding to ω_{sc}

C. Series excitation speed regulation characteristics above base speed ($\omega_r > \omega_{sc}$)

When the motor speed $\omega_r > \omega_{sc} = 6900rpm$, the corresponding data of the speed, output power and output torque obtained from the simulation results are shown in Table 3. The output torque of SRM will decreases by ω_r^{-2} with the decrease of the speed to realize the serial-excitation operation characteristics.

Table 3: Speed and output power of SRM corresponding to $\omega_r > \omega_{sc}$

Rotor Speed	Power Output	Output Torque
7000 rpm	9618.24 W	13.1211 N.m
8000 rpm	8347 W	9.9635 N.m
9000 rpm	7370.38 W	7.82022 N.m
10000 rpm	6605.74 W	6.30801 N.m

The debugging results show that SRM can achieve constant power speed regulation in the range of the speed ω_r of 1500rpm $\sim$ 6900rpm above the base speed, which can reach 2∼3 times of the rated speed, and meet the performance requirements of wide speed regulation range of electric vehicle driving motor.

V. FINITE ELEMENT PARAMETERIZATION OPTIMIZATION OF SRM

The structural parameters optimal design of SRM can improve motor performance and prolong motor life. The Quasi-Newton method is used to optimize the finite element parametric model of SRM in this design. Figure 6 shows the specific optimization steps of finite element optimization.
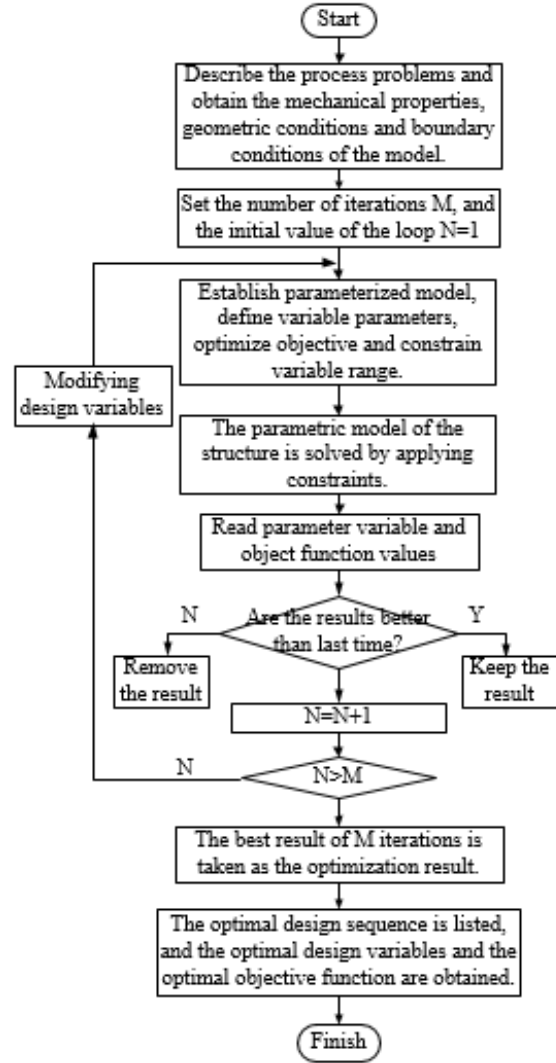
Fig. 6. Specific steps of Quasi-Newton optimization.

A. Optimization performance evaluation index of SRM

Based on the wide speed range characteristics of SRM obtained in previous section, SRM should achieve large working torque and small torque ripple as much as possible under the condition of high efficiency. The optimization performance evaluation indexes of SRM are represented by average torque, torque ripple coefficient and efficiency, which are defined as follows.

(1) Average torque

According to the principle of electromechanical conversion, the average torque T_{av} of SRM when it is in steady state operation is defined as:

$$T_{av} = \frac{1}{\theta} \sum_{k=1}^{m} \int^{(\theta_{on}+\theta_p)} T_k(\theta, i) d\theta, \qquad (10)$$

where θ_p represents the period of phase current, m represents the number of phases, and T_k represents the phase torque and θ_{on} represents the turn-on angle of the switch device. The larger T_{av} is, the higher the average torque of SRM is.

(2) Torque ripple coefficient

The torque ripple of SRM can be characterized by the torque ripple coefficient K_p and is defined as:

$$K_p = \frac{T_{max} - T_{min}}{T_{av}} \qquad (11)$$

where T_{max} is the maxmum of torque, and T_{min} is the minimum of torque. The smaller K_p is, the smaller the torque ripple of SRM is.

(3) Efficiency

SRM roughly includes three kinds of losses, namely, core loss, winding copper loss, additional loss. The total loss of the motor can be obtained after each loss of the motor is solved, and then the efficiency of the motor can be judged. The efficiency of SRM can be characterized by E_i and defined as:

$$E_i = \frac{P_2}{P_2 + P_{core} + P_{Cu} + P_{fw} + P_s} = \frac{T_{av}\omega}{T_{avg}\omega + P_{total}}, \qquad (12)$$

where P_2, P_{core}, P_{Cu}, P_{fw}, P_s and P_{totla} represent output power, core loss, copper loss, mechanical loss, stray loss and total loss respectively [12]. The mechanical loss P_{fw} generally includes the frictional loss and windage loss. The stray loss P_s denotes power loss in semiconductors (diodes and IGBTs), conduction, and switching losses separately [14]. The larger the evaluation index E_i is, the higher the efficiency of SRM.

B. Selection and constraints of design variables

The pole arcs of the stator and rotor of SRM are ones of the important parameters affecting the performance of the motor, the saturation degree of magnetic circuit and the mechanical strength of the rotor. Therefore, the stator pole-arc coefficient ebs and rotor pole-arc coefficient ebr of the motor are selected as the optimization design variables, which can be expressed as:

$$\begin{cases} ebs = \frac{\beta_s}{2\pi/N_s} \\ ebr = \frac{\beta_r}{2\pi/N_r}, \end{cases} \qquad (13)$$

where N_s and N_r are the pole number of the stator and rotor of SRM.

In order to realize the self-starting of the motor, it is necessary to ensure that the adjacent salient poles of the stator and rotor have the overlapping regions when the salient pole axis of the stator and rotor are critically aligned [15]. The pole arcs of the stator and rotor need to meet the following condition [1]:.

$$\begin{cases} min(\beta_s, \beta_r) \geq \frac{2\pi}{mN_r} \\ \beta_s + \beta_r \leq \frac{2\pi}{N_r}. \end{cases} \qquad (14)$$

Based on the mechanical design requirements of the motor and the above constraints, the pole arc coefficients ranges of stator and rotor of the four-phase 8/6 structure SRM are determined. The value ranges of the optimization design variables ebs and ebr are [0.45, 0.65] and [0.35, 0.6], respectively.

C. Torque performance optimization of SRM

ebs and ebr are changed to optimize the average torque and torque ripple [7]. Figure 7 shows the optimized 3D diagram of the average torque and torque ripple of SRM. According to the analysis of Fig. 7 (a) and Fig. 7 (b), when the values of ebs and ebr are 0.55 and 0.4 respectively, $maxT_{av}$ of SRM is 66.3714N.m, and the torque ripple coefficient K_p is 1.37889. When the values of ebs and ebr are 0.5 and 0.45 respectively, $minK_p$ of SRM is 1.35036, and the average torque T_{av} is 66.1522 N.m.

D. Efficiency optimization of SRM

As illustrated in Fig. 8, the efficiency of SRM varies from 84% to 89% with the increase of the optimization design variables ebs and ebr, and both ebs and ebr have a great influence on the motor efficiency. As can be seen from Fig. 8 (a), with the increase of the rotor pole arc coefficient ebr, the efficiency E_i of SRM increases first and then decreases. When ebr is 0.55, $maxE_i = 0.895$. It can be seen from Fig. 8 (b) that the efficiency increases with the increase of the stator pole-arc coefficient ebs.

ebs and ebr are changed to optimize motor efficiency. Figure 9 shows the optimized 3D diagram of the efficiency of SRM. When ebs and ebr are 0.55 and 0.5 respectively, $maxE_i$ of SRM is 89.66%.

E. Multi-objective optimization of SRM

From the results of single objective optimization, the pole-arc coefficients of the stator and rotor have different optimal values respectively, which make the efficiency and average torque maximum and the torque ripple coefficient minimum. Therefore, a multi-objective optimization function is proposed in this paper, which is defined by using three weight factors and three base values. When the multi-objective function is maximized, an appropriate tradeoff among efficiency, average torque, and torque ripple coefficient can be obtained. The multi-objective optimization function can be expressed as:

$$W = \omega_E \frac{E_i}{E_b} + \omega_T \frac{T_{av}}{T_b} + \omega_k \frac{1}{K_p K_b}, \qquad (15)$$

$$T_b = maxTav, \qquad (16)$$
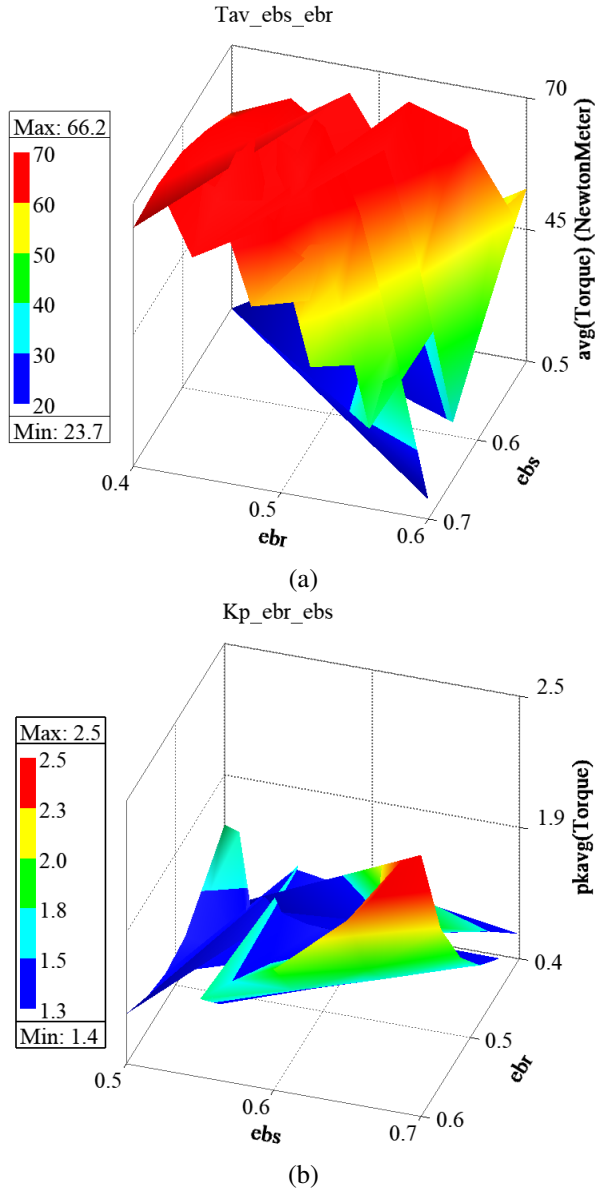
$$K_b = max1/Kp, \qquad (17)$$

(a)

(b)

Fig. 7. Optimized 3D diagram of average torque and torque ripple. (a) Optimized 3D diagram of the average torque. (b) Optimized 3D diagram of torque ripple.

$$E_b = maxE_i, \qquad (18)$$

$$\omega_T + \omega_k + \omega_E = 1, \qquad (19)$$

where, W is the designed multi-objective function, ω_T, ω_K and ω_E are the weighting factors of average torque, torque ripple coefficient and efficiency respectively, whose values are 0.4, 0.4 and 0.2. T_b, K_b, and E_b are the base values of average torque, torque ripple coefficient, and efficiency respectively, and are the maximum values determined by single objective optimization.

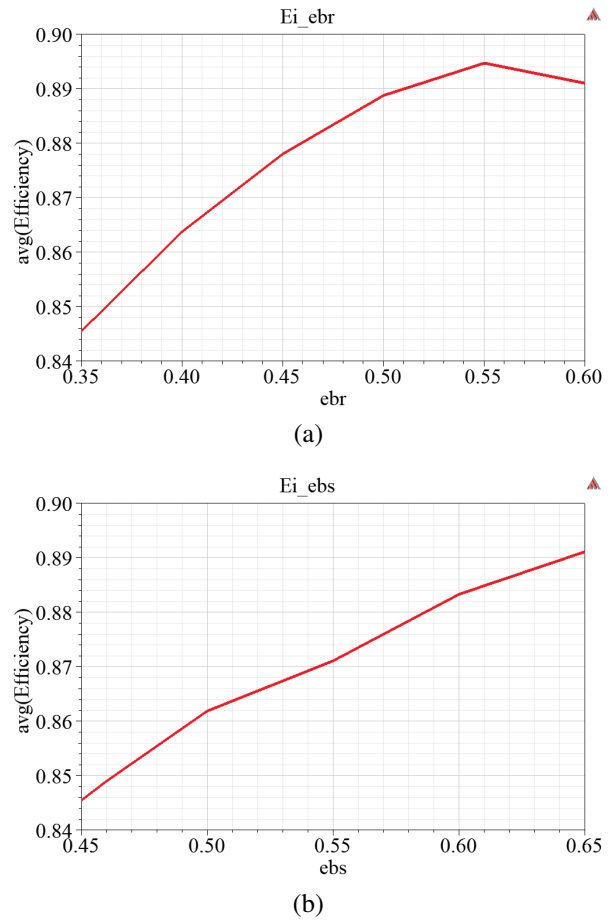According to the multi-objective optimization curve family in Fig. 10, when the values of *ebs* and *ebr* are

(a)

(b)

Fig. 8. Curve family of E_i as a function of optimization variables. (a) Curve of E_i as a function of *ebr*. (b) Curve of E_i as a function of *ebs*.
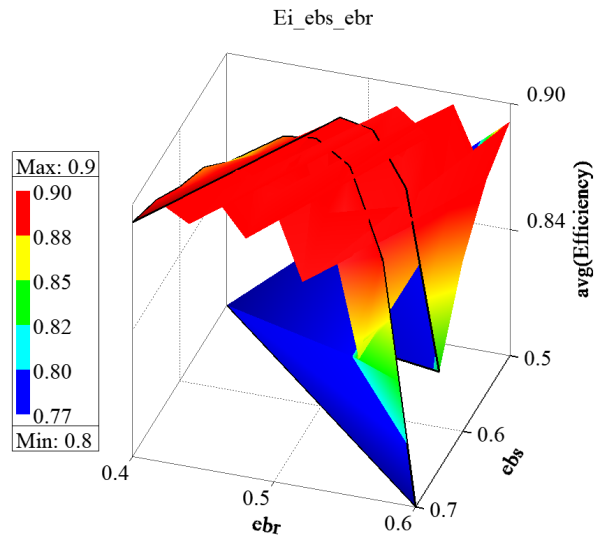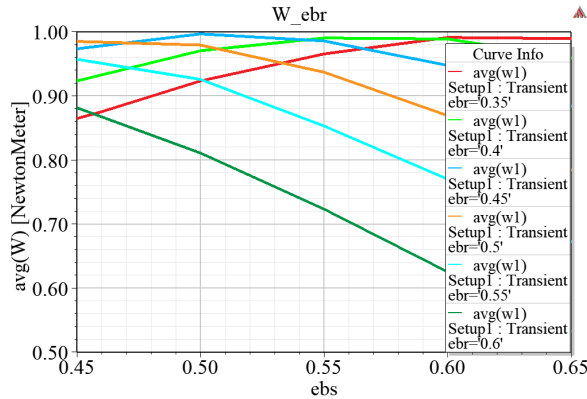

Fig. 9. Optimized 3D diagram of E_i.

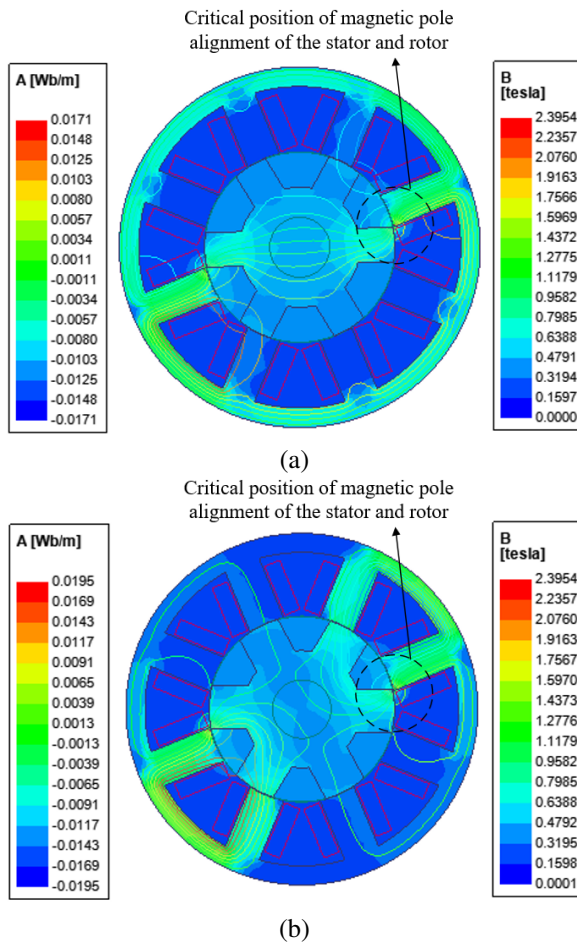Fig. 10. Multi-objective optimization curve family of SRM.

(a)

(b)

Fig. 11. Comparison of magnetic field distribution of SRM before and after optimization. (a) Magnetic field distribution of SRM before optimization. (b) Magnetic field distribution of SRM after optimization.

0.5 and 0.45, respectively, the maximum value *maxW* of the multi-objective weighting function is 0.9958, and

the corresponding objective function values of average torque, torque ripple coefficient, and efficiency are 66.1522 N.m, 1.35036, and 89%.

VI. MOTOR PERFORMANCE COMPARISON BEFORE AND AFTER OPTIMIZATION

The optimized pole-arc parameters of SRM were brought into the motor model, and the limiting current controlled by CCC was reduced to meet the corresponding rated power requirements. Then, the magnetic field distribution, torque characteristics, and efficiency Map calculation results were analyzed and compared between the two motor models before and after optimization in a wide speed range.

A. Comparison of SRM magnetic field distribution before and after optimization

By comparing Fig. 11 (a) and Fig. 11 (b), it can be seen that the flux leakage at the critical position, where the salient poles of the stator and rotor coincide, is significantly reduced after optimization. In addition, the color representing the size of magnetic flux density B is obviously lighter at the pole tip where the salient poles of the stator and rotor coincide, which means that the saturation degree of the magnetic circuit is significantly reduced after optimization, so the torque ripple caused by the switching point in the torque overlap area will be significantly reduced [8].

B. Comparison of torque characteristics before and after optimization

The average torque and torque ripple coefficient were calculated in the time range of 2ms~8ms. The comparison of torque characteristics before and after optimization is shown in Fig. 12.

The average torque decreases slightly before and after optimization, but the ripple coefficient decreases greatly from 1.2093 to 0.8965, which proves that increasing the stator and rotor pole-arc coefficients of SRM can improve the torque ripple performance of the motor effectively [16].
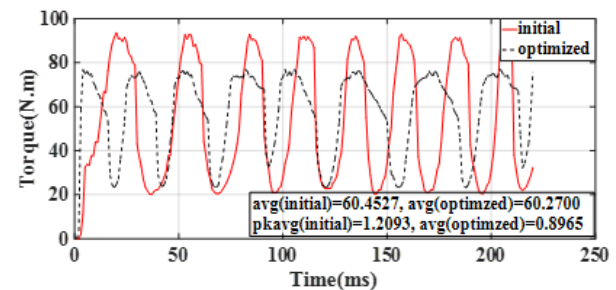

Fig. 12. Torque comparison of the motor model before and after optimization.

C. Efficiency comparison before and after optimization

The RMxprt model rated load performance comparison of SRM before and after optimization is shown in Table 4. Due to the obvious reduction of copper loss in the optimized model, the motor efficiency is increased from 89.9% to 91.5%, which proves that the stator and rotor pole arc coefficients also have a great impact on the motor efficiency.

Table 4: Comparison of efficiency at rated load before and after pole arc coefficient optimization of SRM

Indicators	Initial	Optimized
Iron loss (W)	282.578	314.449
Copper loss (W)	895.011	685.805
Efficiency (%)	89.9018	91.4525

D. Comparison of speed range before and after optimization

The stator and rotor pole-arc coefficients of SRM are increased, and the lower and upper limits of chopper current are adjusted to 69 and 71, to keep the rated output power almost the same before and after optimization. According to the comparison of the two output power
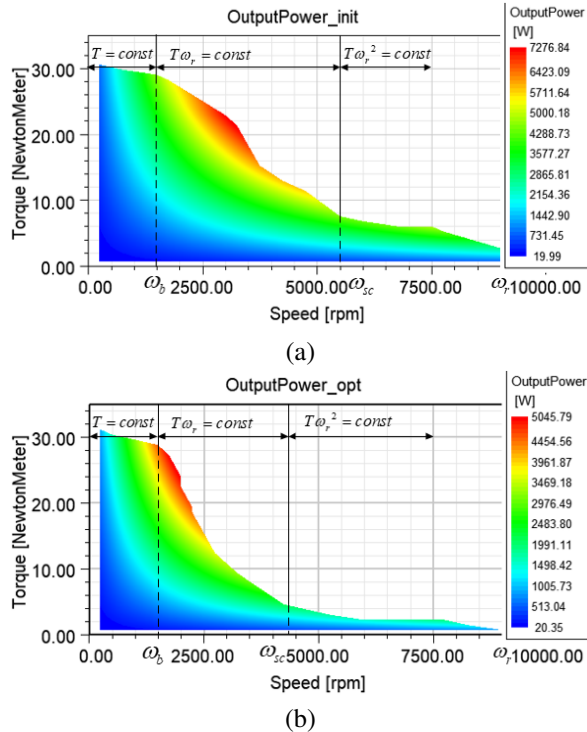

(a)

(b)

Fig. 13. Comparison of output power Map calculation of motor model before and after optimization. (a) SRM output power Map before optimization. (b) Output power Map of SRM after optimization.

map calculations of the motor model in Fig. 13, the constant power speed range of the motor is reduced after optimization, but the highest speed ω_{sc} in the constant power region is still satisfied with 2 to 3 times of the rated speed, which can fully meet the operation requirements of the wide speed regulation range for the driving motor in EV.

VII. CONCLUSION

Because SRM has the advantages of large starting torque, wide speed range, strong load capacity, and high efficiency, it is especially suitable for new energy vehicle driving. According to the design requirements of the new energy vehicle drive, a 10 kW 8/6 structure SRM motor model is designed, and the wide speed range debugging of the motor model and the optimization of the motor performance based on parametric modeling is completed in this paper.

It can be seen from the performance comparison of the SRM model before and after optimization that the average torque of the optimized SRM model is basically unchanged, but the torque ripple coefficient is greatly reduced under the condition of meeting the design power requirements. The optimization of motor structure parameters also plays a role in optimizing the efficiency of the motor. The comparison of the output power Map before and after optimization shows that the increase of the pole-arc coefficients makes the constant power range of the motor smaller, but it can better meet the requirements of electric vehicles for the speed range. In the future, more structural parameters of the motor should be considered, and more performance optimization should be realized, including power density, vibration noise, etc.

REFERENCES

[1] Y. Y. Zhu, C. T. Yang, and Y. Yue, "Design and optimisation of an in-wheel switched reluctance motor for electric vehicles," *IET Intelligent Transport Systems*, vol. 13, no. 2, pp. 175-182, 2019.

[2] H. Cheng, H. Chen, and Z. Yang, "Design indicators and structure optimization of switched reluctance motor for electric vehicles," *IET Electric Power Application*, vol. 9, no. 4, pp. 319-331, 2015.

[3] A. A. Memon, M. M. Shaikh, S. S. H. Bukhari, and J. -S. Ro, "Look-up data tables-based modeling of Switched Reluctance Machine and experimental validation of the static torque with statistical analy-

sis," *Journal of Magnetics*, vol. 25, no. 2, pp. 233-244, 2020.

[4] X. D. Sun, K. K. Diao, and G. Lei, "Direct torque control based on fast modeling method for a segmented-rotor switched reluctance motor in HEV application," *IEEE Journal of Emerging and Selected Topics in Power Electronics*, vol. 9, no. 1, pp. 232-241, Feb. 2021.

[5] F. E. Fleming and C. S. Edrington, "Real-time emulation of switched reluctance machines via magnetic equivalent circuits," *IEEE Transactions on Industry Magnetic*, vol. 63, no. 6, pp. 3366-3376, June. 2016.

[6] C. Ma and L. Y. Qu, "Design considerations of switched reluctance motors with bipolar excitation for low torque ripple applications," *IEEE Energy Conversion Congress and Exposition*, Denver, CO, USA, pp. 926-933, 2013.

[7] J. Q. Chen, H. L. Xian, and F. C. LAN, "Structural torque ripple suppression method for switched reluctance motor," *Journal of Mechanical Engineering*, vol. 56, no. 20, pp. 106-119, Oct. 2020.

[8] Z. Li, L. Zheng, and W. Yang, "Research on torque ripple and structure optimization design of switched reluctance motor," *Electric Machines and Control*, vol. 22, no. 6, pp. 11-21, Jun. 2018.

[9] X. D. Xue, K. W. E. Cheng, and J. K. Lin, "Optimal control method of motoring operation for SRM drives in electric vehicles," *IEEE Transactions On Vehicular Technology*, vol. 59, no. 3, pp. 1191-1204, Mar. 2010.

[10] H. H. Wang, *Speed Control Technology of Switched Reluctance Motor*, China Machine Press, Beijing, Apr. 2014.

[11] L. J. Liu, M. W. Zhao, and X. B. Yuan, "Direct instantaneous torque control system for switched reluctance motor in electric vehicles," *J. Eng*, vol. 2019, no. 16, pp. 1847-1852, 2019.

[12] H. X. Wu, *Theory and Control Technology of Switched Reluctance Motor System*, China Electric Power Press, Beijing, Jul. 2010.

[13] J. W. Zhang, H. H, Wang, and L. Chen, "Multi-objective optimal design of bearingless switched reluctance motor based on multi-objective genetic particle swarm optimizer," *IEEE Transactions on Magnetics*, vol. 54, no. 1, Jan. 2018.

[14] A. A. Memon, S. S. H. Bukhari, and J. -S. Ro, "Experimental determination of equivalent iron loss resistance for prediction of iron losses in a Switched Reluctance Machine," *IEEE Transactions on Magnetics*, vol. 58, no. 2, pp. 1-4, Feb. 2022.

[15] B. Anvari, H. A. Toliyat, and B Fahimi, "Simultaneous optimization of geometry and firing angles for in-wheel switched reluctance motor drive," *IEEE Transactions on Transportation Electrification*, vol. 4, no. 1, pp. 322-329, Mar. 2018.

[16] X. M. Deng, R. Li, L. Hao, A. K. Zhang, and J. H. Zhou, "Design and finite element analysis of a novel permanent magnet assisted reluctance synchronous motor," *Applied Computational Electromagnetics Society (ACES) Journal*, vol. 35, no. 9, pp. 1012-1021, Sep. 2020.

Lijun Liu was born in Shanxi, China, in 1977. She received her M.S. degree in Power Electronics and Power Drive from China University of Mining and Technology, Xuzhou, China, in 2006, and is currently pursuing a Ph.D. degree in Power Electronics and Power Drive from Shanghai University, Shanghai, China.

She is currently a lecturer at the School of Electrical Engineering and Automation, Jiangsu Normal University, Xuzhou, China. She has published more than 10 articles. Her research interests include the design and optimization of new energy-electric drive systems, and industrial motion control systems, etc.

Yu Huang was born in Jiangsu, China. He received his B. S. degree in Electric Engineering from Jiangsu Normal University, Xuzhou, China, in 2022, and is currently pursuing an M.S. degree in Power Systems from North China Electric Power University, Baoding, China. His research interests include the design and optimization of new energy electric drive systems, and high voltage techniques, etc.

Mingwei Zhao was born in Shandong China, in 1975. He received an the M.S. degree in Power Electronics and Power Drive from Nanjing University of Aeronautics and Astronautics, Nanjing, China, in 2012, and is currently pursuing a Ph.D. degree in Control Science and Control Engineering from Shanghai University, Shanghai, China.

Since 2006, he has been an experiment lecturer with the school of Electrical Engineering and Automation, Jiangsu Normal University, Xuzhou, China. He is the author of 10 articles. His research interests include the robot dynamic drive and cooperative control, and industrial motion control system, etc.

Yi Ruan was born in Shanghai, China, in 1955. He received an M.S. degree in Shanghai University of Technology, Shanghai, China, in 1989, and a Ph.D. degree in Power Electronics and Power Drive from Shanghai University, Shanghai, China, in 1996.

From1989 to 2015, he has been a professor of the Electromechanical Engineering and Automation, Shanghai University, Shanghai, China. He once served as the chairman of the Special Committee Of Variable Frequency Power Supply And Electric special committee of variable frequency power supply and electric drive of the Power Supply Society of China. His research interests include the power electronics and power drive, control and power conversion technology of new energy, etc.